Available online at www.sciencedirect.com
SCIENCE DIRECT®
Journal of Magnetic Resonance 162 (2003) 133–140
JMR Journal of Magnetic Resonance
www.elsevier.com/locate/jmr

Spectral restoration from low signal-to-noise, distorted NMR signals: application to hyphenated capillary electrophoresis-NMR

Yu Li,[a,b] Michael E. Lacey,[b,c] Jonathan V. Sweedler,[b,c] and Andrew G. Webb[a,b,d,*]

[a] *Department of Electrical and Computer Engineering, University of Illinois at Urbana-Champaign, Urbana, IL 61801, USA*
[b] *Beckman Institute for Advanced Science and Technology, University of Illinois at Urbana-Champaign, Urbana, IL 61801, USA*
[c] *School of Chemical Sciences, University of Illinois at Urbana-Champaign, Urbana, IL 61801, USA*
[d] *Physikalisches Institut, Universitaet Wuerzburg, Germany*

Received 22 July 2002; revised 11 February 2003

Abstract

In capillary electrophoresis separations coupled to NMR signal detection using small solenoidal coils, electrophoretic currents cause substantial distortion in the NMR spectral linewidths and peak heights, distortions which cannot be fully counteracted through shimming. The NMR spectra also have a low signal-to-noise ratio due to the small amounts of material, typically <1 nmol, associated with such microseparations. This study proposes a two-step, signal processing method to restore spectral lines from the distorted NMR spectrum. First, a reference signal is acquired to estimate the broadening function, as a combination of several Lorentzian functions, using a gradient descent method. Then multi-resolution wavelet analysis is applied to the distorted spectrum to determine an initial estimate of the frequencies of the spectral lines. Convergence to the final spectrum, a second set of Lorentzians, involves deconvolution with the estimated broadening function using a gradient descent method. Experimental CE-NMR data show that considerable improvements in spectral quality are possible using this approach, although fine splittings can not be resolved if the broadening function is large.

Keywords: Capillary electrophoresis; Hyphenated NMR detection; Wavelets; Deconvolution; Lineshape distortion

1. Introduction

High spectral resolution in nuclear magnetic resonance (NMR) experiments is needed for the accurate quantitation of signal intensities, chemical shifts and scalar couplings that can be used to identify and/or confirm the structures of unknown compounds. This requirement corresponds to a static magnetic field (B_0) homogeneity over the sample of between 0.01 and 0.001 parts per million (ppm) for most liquid-state NMR experiments. In high-resolution NMR studies, careful sample preparation and shimming enable this level of B_0 homogeneity to be achieved. In many cases, however, the spectral linewidth is still dictated by the apparent transverse relaxation time (T_2^*) of the sample rather than the true spin–spin relaxation time (T_2). Various methods exist for deconvolving the effects of the inhomogeneous static magnetic field. The most widely used method is termed "reference deconvolution" [1–10], a technique which can produce substantial improvements in spectral resolution if a suitable reference peak or spectrum is available.

One relatively recent application, in which broad, distorted NMR linewidths can interfere substantially with spectral interpretation, irrespective of the intrinsic B_0 homogeneity, is the hyphenation of capillary electrophoresis (CE) separations with NMR detection [11–18]. In these experiments, separations are carried out in capillaries with typical inner diameters of 75 μm or less. The separation process in CE involves application of a large voltage across the ends of a buffer-filled capillary, which produces a current (10–90 μA) through the sample [19,20]. In the most traditional form of CE, analytes separate according to their respective charge-to-size ratios. Very low limits of NMR detection have been

* Corresponding author. Fax: 1-217-244-0105.
E-mail address: a-webb2@uiuc.edu (A.G. Webb).

1090-7807/03/$ - see front matter © 2003 Elsevier Science (USA). All rights reserved.
doi:10.1016/S1090-7807(03)00055-7

achieved using small (~250 μm diameter) solenoidal radiofrequency (RF) coils, with high filling factors. However, since the solenoidal coil is oriented perpendicular to the direction of B_0, the current through the sample generates a magnetic field gradient, $\partial B_z/\partial x$, across the sample, given by Ampere's law

$$\frac{\partial B_z}{\partial x} \propto \frac{I}{r_0^2}, \tag{1}$$

where x represents the direction of the long axis of the capillary, I is the current that passes through the sample, and r_0 is the inner radius of the capillary. The magnitude of the induced magnetic field gradient, for currents greater than about 10 μA, means that the NMR lines are distorted substantially. One method to overcome the spectral distortion is to use "periodic stopped-flow" CE-NMR, in which the voltage is switched off during data acquisition [16]. This approach, however, requires prior knowledge of analyte migration times or a sufficiently high signal-to-noise ratio (SNR) to enable continuous monitoring in order to determine the exact time at which to switch off the current. Furthermore, separation efficiency may decrease as a result of the periods of stopped flow. An alternative approach is to use a vertically oriented capillary within a coil of "saddle" geometry. In this case, no magnetic field gradients exist within the sample, but the use of the intrinsically lower-sensitivity saddle geometry [21], together with the much smaller filling factors for even the smallest saddle coils, result in poorer limits of detection than size-matched solenoids. This paper explores whether post-processing of the CE-NMR spectrum, acquired using a high sensitivity solenoid coil, can at least partially restore spectral resolution.

NMR post-processing methods can be categorized into two classes: linear and nonlinear. The advantages of linear methods, including reference deconvolution, are the relative simplicity of implementation, and the fact that any artifacts introduced into the processed spectra are well-characterized, and can therefore be easily recognized. The main disadvantages relate to the results being limited by the information inherent in the input data. In comparison, nonlinear algorithms such as maximum entropy, Bayesian analysis and the technique proposed in this paper are more complicated to implement, and spectral artifacts are not well-characterized, thus leading to an increased possibility of spectral misinterpretation. However, the potential advantage of nonlinear processing methods is the ability to incorporate prior knowledge, irrespective of the quality of data actually acquired.

In this study, the experimentally acquired NMR spectrum is mathematically modeled as the frequency-domain convolution of the "ideal" spectrum and a smooth broadening function produced by the CE current. In similar fashion to the reference deconvolution technique, reference signals are acquired under both static (no applied voltage) and dynamic (applied voltage) conditions. A gradient descent method is ultimately used to estimate the system broadening function from the reference signals, and then the "ideal" spectrum is estimated from this broadening function and the experimental CE-NMR spectrum. However, in the case of spectra with a very low SNR, common for CE-NMR hyphenation, the convergence of this type of algorithm is highly dependent upon the initial parameters used. In our proposed scheme, the gradient descent convergence algorithm is initialized by multiresolution detection via a wavelet transform (WT) of the acquired data, a process which estimates the frequency locations of the spectral lines in the distorted CE-NMR spectrum. Even though only the initialization part of the entire algorithm utilizes this technique, it plays a key role in achieving the convergence of the NMR parameters including the chemical shifts, spectral line intensities and linewidths. Processing of CE-NMR spectra demonstrates that this overall technique achieves comparable spectral restoration to simpler techniques such as reference deconvolution when the SNR of the distorted spectrum is high, but gives considerable improvements in performance when the SNR is low. Thus, this method is particularly well suited to CE-NMR.

2. Experimental

2.1. System model

A noise-free NMR spectrum, $S_e(f)$, consisting of Lorentzian lines can be written as

$$S_e(f) = \sum_{i=1}^{K} \frac{A_i \alpha_i}{\alpha_i^2 + (f - f_i)^2}, \tag{2}$$

where K is the number of Lorentzian lines, and A_i is the amplitude, α_i the damping constant and f_i the frequency, respectively, of the ith peak. The spectral distortion process is modeled as a linear convolution in the frequency domain. Thus, the degraded spectrum, $S_{eb}(f)$, is given by

$$S_{eb}(f) = S_e(f) \ * \ B(f) + N_{eb}(f), \tag{3}$$

where $B(f)$ is the broadening function, which is assumed to be a smooth function, and $N_{eb}(f)$ is the contribution from white noise. If a reference signal is acquired, the reference signals in the absence of, $S_r(f)$, and in the presence of, $S_{rb}(f)$, spectral distortion are related by the linear convolution:

$$S_{rb}(f) = S_r(f) \ * \ B(f) + N_{rb}(f), \tag{4}$$

where $N_{rb}(f)$ also represents white noise. In CE-NMR, $S_r(f)$ can be obtained before the voltage is applied as a

spectrum of the buffer used as the mobile phase in the separation. For example, $S_r(f)$ corresponds either to the peak from water in protonated buffers or the residual HOD peak in deuterated buffers. $S_{rb}(f)$ is then obtained by switching on the voltage. Since it takes some time for the constituents of the separation to travel from the CE separation column to the NMR detection cell, the first few spectra acquired contain signal from the buffer only. At appropriate migration times after the voltage has been turned on, spectra, $S_{eb}(f)$, are acquired which correspond to the individual components of the initial mixture.

Using Eq. (4), the broadening function $B(f)$ can be estimated from $S_r(f)$ and $S_{rb}(f)$. Then, using Eq. (3), $S_e(f)$ can be restored from $S_{eb}(f)$ and the estimated system broadening function $B(f)$. A basic assumption in this study is that $B(f)$ is of the same form as $S_e(f)$. Specifically, the distortion function is given by

$$B(f) = \sum_{i=1}^{L} \frac{A_{b,i}\alpha_{b,i}}{\alpha_{b,i}^2 + (f - f_{b,i})^2}, \tag{5}$$

where L is the number of the Lorentzian lines and $A_{b,i}$, $\alpha_{b,i}$, and $f_{b,i}$ are the amplitudes, damping constants, and center frequencies of these Lorentzian lines, respectively. The discrete form of this equation is equivalent to an autoregressive (AR) model [22] with the value of L being the model order. This assumption is valid because the expression in Eq. (5) is able to represent most regular smooth functions if L is large enough. It is also convenient to make such an assumption in that the same estimator can be applied to both $B(f)$ and $S_e(f)$. Based on the model expressions in Eqs. (2) and (5), the aim of this study is equivalent to looking for the optimum estimator of the spectral parameters $\{A_i, \alpha_i, f_i\}$ given the experimental data $\{S_{eb}, S_r, S_{rb}\}$. The parameter estimator uses the gradient descent method. The parameters $\{A_{b,i}, \alpha_{b,i}, f_{b,i}\}$ and $\{A_i, \alpha_i, f_i\}$ for $B(f)$ and $S_e(f)$, respectively, are adjusted to minimize a defined error function. Theoretically, if the error function is quadratic in terms of the parameters, the algorithm will converge eventually to the optimum values of these parameters. However, this is often not true in practice. The error function often converges to local minima if the initial values of the parameters are not close enough to the optimum. Furthermore, it can be shown that the Lorentzian nature of the NMR spectrum makes the convergence of the algorithm very sensitive to the initialization of the frequency parameters $\{f_i\}$. Therefore, a method is necessary to give a good initial parameter estimate of the respective $\{f_i\}$ from the low SNR, highly distorted CE-NMR spectrum. Our approach is to use multi-resolution wavelet processing to provide an initial estimate of the frequency locations of the spectral peaks to facilitate the convergence of the gradient descent method.

2.2. Multi-resolution wavelet estimation of spectral frequencies

WT analysis has drawn much attention in NMR data processing recently. An early paper proposed two iterative procedures, obtained from wavelet analysis, to quantify the chemical shift, apparent relaxation time, resonance amplitude, and phase of NMR spectra [23]. In later research, Barache et al. [24] developed an analytical tool to remove a large undesired spectral line, and to correct for phase distortions in a signal, caused by eddy currents, using the continuous wavelet transform (CWT). Two more recent studies focused on the issues of improving NMR spectral resolution. One applied CWT analysis to solid NMR spectra [25]: the other implemented a discrete wavelet transform (DWT) method to improve spectral resolution in liquid-state NMR [26].

Multi-resolution detection with wavelets in this study is a CWT analysis derived from Mallat's theory in 1992 [27]. A wavelet, $\Psi(f)$, with two vanishing moments can be written as [28]

$$\Psi(f) = -\frac{\mathrm{d}^2\theta(f)}{\mathrm{d}f^2}, \tag{6}$$

where $\theta(f)$ is a perfectly smooth function with a fast decay, which reaches a maximum value at $f = 0$. The wavelet transform, $W_{S_{eb}}(s, f)$, of the distorted spectrum is given by

$$\begin{aligned} W_{S_{eb}}(s,f) &= S_{eb} * \psi_s(f) \\ &= -(S_e * B + N_{eb}) * s^2 \frac{\mathrm{d}^2\theta_s(f)}{\mathrm{d}f^2} \\ &= -s^2 \frac{\mathrm{d}^2 S_e(f)}{\mathrm{d}f^2} * B * \theta_s(f) - W_{N_{eb}}, \end{aligned} \tag{7}$$

where $W_{N_{eb}}$ is the wavelet transform of the white noise and s is the scale factor. Because both B and θ are smooth, the convolution of these two functions yields a new smooth function. Thus, the wavelet transform of the distorted spectrum is equal to the product of the square of the scale factor and the convolution of a smooth function with the negative second derivative of the original spectrum without distortion. From Eq. (2), the second derivative of S_e is

$$\frac{\mathrm{d}^2 S_e(f)}{\mathrm{d}f^2} = \sum_{i=1}^{K} \frac{6A_i\alpha_i(f - f_i)^2 - 2A_i\alpha_i^3}{[(f - f_i)^2 + \alpha_i^2]^3}. \tag{8}$$

Then the third derivative is

$$\frac{\mathrm{d}^3 S_e(f)}{\mathrm{d}f^3} = \sum_{i=1}^{K} \frac{-2A_i\alpha_i[f - f_i][(f - f_i)^2 - \alpha_i^2]}{[(f - f_i)^2 + \alpha_i^2]^4}. \tag{9}$$

Zeros occur in the third derivative of the original spectrum at $f = f_i$, $i = 1, 2, \ldots, K$, with these zeros corresponding to the minima of the second derivative, or the

maxima of the negative second derivative. Accordingly, a search for the extrema of Eq. (8) detects the frequency location of the spectral line peaks $\{f_i,\ i = 1, 2, \ldots, K\}$. Since convolution with a fast decaying smooth function does not affect the position of the extrema, the local maxima of the wavelet transform of S_{eb} correspond to the maxima of the negative second derivative of S_e if a wavelet-satisfying Eq. (6) is applied. Thus, the frequency parameters $\{f_i,\ i = 1, 2, \ldots, K\}$ of the desired spectrum can be determined by detecting the local maxima of the wavelet transform of the distorted NMR spectrum. In practice, the distortion in the experimentally acquired data introduces a frequency shift, since the maximum point of the smooth function is not at its center. However, this effect is frequency independent and hence can be removed by calibration with a reference signal.

There are two requirements for the choice of the wavelet. First, the wavelet must have two vanishing moments. Second, the wavelet must be equal to the negative second derivative of a smooth function with a rapid decay. The "Mexican hat" [28], the negative second derivative of a Gaussian function, is chosen as the wavelet function in this study. The wavelet transform of the acquired NMR spectrum can be processed as a two-dimensional function of the scale s and the frequency f. The maxima of the wavelet transform occur exactly at the locations of the peaks of the original spectrum if the scale range is appropriate. The search for the maxima of the wavelet transform is performed using a "maximal line," i.e., a two-dimensional plot of the local maxima of wavelet transforms performed at different scales, as a function of scale and frequency. The two-dimensional structure of these maxima lines aids differentiation between true spectral peaks and those corresponding to noise (assumed to be white in this study). According to Mallat, the expected value of the magnitude of the wavelet transform of white noise is inversely proportional to the scale s [28]. In contrast, the magnitude of the wavelet transform of the original spectrum is proportional to the square of the scale s at a fixed frequency as shown in Eq. (7). Moreover, the continuity of the maxima lines caused by noise will be poor because of its inherent randomness, while the maxima lines of the real spectral line peaks extend over a large range of scales. Thus, the evolution of the maxima lines of the original spectrum can be detected to differentiate between true spectral lines and those from white noise.

2.3. The gradient descent method

The gradient descent method [29] is applied to estimate the system line broadening function from the reference signal, and also to produce the deconvolved spectrum from the degraded CE-NMR data. The error functions for the line broadening estimator (ε_b) and the deconvolved spectrum estimator (ε_s) are defined by:

$$\begin{aligned}\varepsilon_b &= \sum_{k=1}^{N}[e_b(k)]^2 = \sum_{k=1}^{N}[S_{rb}(k) - S_r\ *\ B(k)]^2,\\ \varepsilon_s &= \sum_{k=1}^{N}[e_s(k)]^2 = \sum_{k=1}^{N}[S_{eb}(k) - S_e\ *\ B(k)]^2,\end{aligned} \tag{10}$$

where k is the sampling index in the frequency domain and N is the number of sampled data points. Experimentally, the spectra S_r, S_{rb}, and S_{eb} are known vectors. The quantities B and S_e can be explicitly expressed in terms of the unknown parameters $\{A_{b,i}, \alpha_{b,i}, f_{b,i}\}$ and $\{A_i, \alpha_i, f_i\}$:

$$\begin{aligned}B(k) &= \sum_{i=1}^{L}\frac{A_{b,i}\alpha_{b,i}}{\alpha_{b,i}^2 + (k\Delta f - f_{b,i})^2},\\ S_e(k) &= \sum_{i=1}^{K}\frac{A_i\alpha_i}{\alpha_i^2 + (k\Delta f - f_i)^2},\end{aligned} \tag{11}$$

where Δf is the digital resolution in the frequency domain and k is the sample index. As outlined previously, multiresolution detection via a wavelet transform gives an estimation of the frequencies of the distortionless spectrum. The other unknown parameters, $\{A_{b,i}, \alpha_{b,i}, f_{b,i}, A_i, \alpha_i\}$ reach their optimum values as the error functions are minimized. Accordingly, the negative gradient of the error functions with respect to the unknown parameters gives the optimized direction leading to minimum errors for any initial values of the parameters. The corresponding update equations for the two estimators are given by:

$$\begin{aligned}A_{b,i}(n+1) &= A_{b,i}(n) + 2u\sum_{k=1}^{N}e_b(k)\sum_{n=1}^{N}S_r(n)\\ &\quad\frac{\alpha_{b,i}}{\alpha_{b,i}^2 + ((k-n)\Delta f - f_{b,i})^2}, \quad i = 1, \ldots, L,\\ \alpha_{b,i}(n+1) &= \alpha_{b,i}(n) + 2u\sum_{k=1}^{N}e_b(k)\sum_{n=1}^{N}S_r(n)\\ &\quad\frac{A_{b,i}[((k-n)\Delta f - f_{b,i})^2 - \alpha_{b,i}^2]}{[\alpha_{b,i}^2 + ((k-n)\Delta f - f_{b,i}^2)]^2}, \quad i = 1, \ldots, L,\\ f_{b,i}(n+1) &= f_{b,i}(n) + 2u\sum_{k=1}^{N}e_b(k)\sum_{n=1}^{N}S_r(n)\\ &\quad\frac{2A_{b,i}\alpha_{b,i}((k-n)\Delta f - f_{b,i})}{[\alpha_{b,i}^2 + ((k-n)\Delta f - f_{b,i}^2)]^2}, \quad i = 1, \ldots, L,\\ A_i(n+1) &= A_i(n) + 2u\sum_{k=1}^{N}e_s(k)\sum_{n=1}^{N}B(n)\\ &\quad\frac{\alpha_i}{\alpha_i^2 + ((k-n)\Delta f - f_i)^2}, \quad i = 1, \ldots, K,\\ \alpha_i(n+1) &= \alpha_i(n) + 2u\sum_{k=1}^{N}e_s(k)\sum_{n=1}^{N}B(n)\\ &\quad\frac{A_i[((k-n)\Delta f - f_i)^2 - \alpha_i^2]}{[\alpha_i^2 + ((k-n)\Delta f - f_i)^2]^2}, \quad i = 1, \ldots, K,\end{aligned} \tag{12}$$

where u is the update step length. The distortion function B is given by the first estimator using the first three update equations. Ideally, if the error functions are quadratic in terms of the parameter vectors, the gradient descent method will work perfectly and the parameters will converge to the optimum values from any initial point with an appropriate update step length. However, in the real case, where the squared error functions are not exactly quadratic and noise exists in the system, the squared error function may converge to a local minimum if the initial values are not close enough to the global minimum point. Therefore, it is important to initialize the parameters as close as possible to the global minimum point before running the algorithm. In particular, the value of the initial f_i's has a significant effect on the convergence, which is why it is important to use the multi-resolution wavelet approach.

The convergence of the gradient descent method is always a matter of practical concern in real applications. If the update step length is large, oscillation around the optimum parameter values will occur. On the other hand, the algorithm takes significant time to converge if the update step length is small [9]. A scheme using a variable update step length is used in this study. The update step length is adjusted at each updating cycle based on the convergence situation. If the square error function drops dramatically, the update length will increase. If the square error function remains the same for a long time, the update step will keep decreasing until it reaches a minimum limit, which is used to end the convergence. This updating technique improves convergence without requiring extensive computational time.

The parameters for the broadening function and the deconvolved spectrum are not initialized in the same manner because of the different requirements for the two cases. The broadening function is required only to be smooth in the system model and thus the convergence constraint is simply that no singularities occur in the final result. There may be multiple solutions which can simulate satisfactorily the real distortion process. For this reason, the parameters $\{A_{b,i}, \alpha_{b,i}, f_{b,i}\}$ are not required to be initialized as stringently as $\{A_i, \alpha_i, f_i\}$.

3. Results

All experiments were performed on a wide-bore (89 mm) magnet (Oxford Instruments) with an Inova (Varian, Palo Alto, CA) console operating at 500 MHz. CE spectra were acquired using a hyphenated CE-NMR setup similar to described previously [16,30] with the particular coil consisting of a 17-turn solenoid, outer diameter 340 μm, wrapped on a polyimide sheath of 20 μm thickness. A capillary of inner diameter 75 μm and outer diameter 230 μm was fed through the polyimide sheath and inserted into the inlet and outlet vials. A voltage was applied across the ends of the capillary using a DC power supply. The sample used to test the proposed algorithm was a solution of 100 mM sucrose in D_2O. Sucrose is representative of a medium sized organic molecule, and the NMR spectrum contains both well-defined simple spectral patterns such as the upfield doublet from the anomeric protons, and also complex multiplet patterns in the aliphatic region. As such, it serves as a good model compound.

A high-resolution spectrum of sucrose obtained in the absence of a CE current is shown in Fig. 1a. The full-width-half-maximum (FWHM) linewidth of the residual HOD resonance was 4.3 Hz. The CE current was then applied and distorted spectra were acquired with different values of the CE current. The triplet structure, located at 4.12 ppm, was used for initial testing of the algorithm because it contains close, overlapping peaks and thus proves challenging to the deconvolution algorithm. Three distorted spectra of the triplet, with electrical current values of 20, 30, and 40 μA, are shown in Fig. 1b. It can be seen that the line broadening and SNR degradation becomes stronger when the CE current

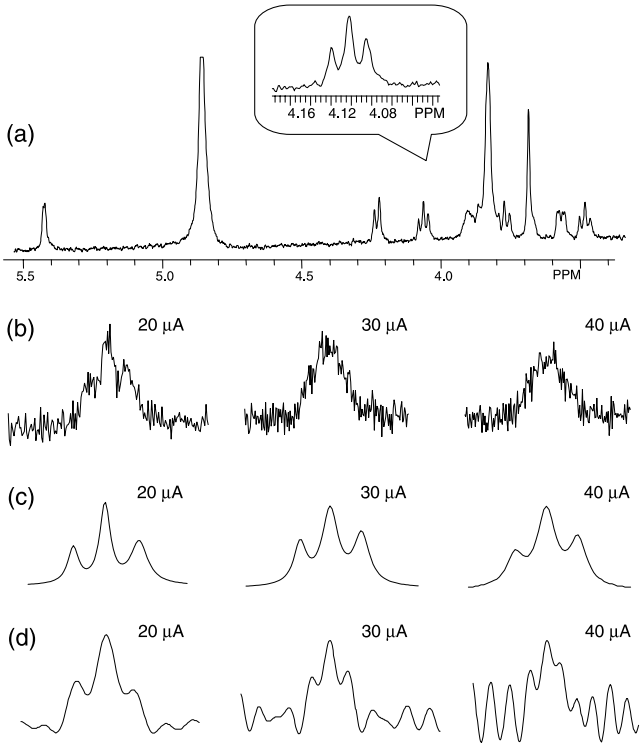

Fig. 1. Spectral deconvolution using a solution of 100 mM sucrose in D_2O. (a) Spectrum acquired without CE current. (b) Distorted spectra acquired with different values of the CE current. An expanded view of the triplet from (a) is shown. (c) Spectral deconvolution results obtained using the method outlined in this paper. (d) Spectra obtained using the reference deconvolution method with a target linewidth of 4.3 Hz, and a spectral window of 40 Hz to define the limits of the HOD peak.

increases. Fig. 1c shows the results of the combined multi-resolution wavelet/gradient descent algorithm. For each value of the current it is possible to discern the multiplet structure, albeit with some amplitude distortions in the individual components of the triplet structure. As a comparison, Fig. 1d shows results using the method of reference deconvolution, using the water line as the reference. Reference deconvolution can be described mathematically as:

$$S_{\mathrm{comp}}(f) = F\left\{ \frac{s_{\mathrm{exp}}(t)s_{\mathrm{ideal}}(t)}{s_{\mathrm{ref}}(t)} \right\}, \tag{13}$$

where $S_{\mathrm{comp}}(f)$ is the deconvolved spectrum, $s_{\mathrm{exp}}(t)$ is the experimentally acquired data corresponding to a distorted spectrum, $s_{\mathrm{ideal}}(t)$ is the time-domain representation of the desired Lorentzian linewidth, and $s_{\mathrm{ref}}(t)$ corresponds to the signal from the reference peak only. The target linewidth for reference deconvolution was 4.3 Hz. At the low CE current value of 20 μA, the two techniques result in similar restoration of the multiplet structure, and one might well prefer to use the more simple reference deconvolution algorithm. As the CE current is increased and the SNR is reduced, the results from reference deconvolution become more difficult to interpret because of ringing artifacts, suggesting that in situations where the spectra are both severely distorted and have a low SNR, more sophisticated deconvolution algorithms, such as the one outlined in this paper, may be needed. It should be noted that a broader target linewidth for the reference deconvolution algorithm would result in lower ringing artifacts, at the expense of spectral broadening, and that incorporation of a Lorentz-to-Gauss transformation could also narrow the spectrum resulting from reference deconvolution.

Individual steps in the processing are shown in Fig. 2. Fig. 2a shows an expanded region of the broadened triplet of sucrose corresponding to a CE current of 20 μA. Also shown are wavelet transforms of the data at different scales. The choice of the range of scale factors is a trade-off between spectral resolution and denoising. A larger scale factor increases the effective denoising but results in poorer spectral resolution in the processed data. For spectral resolutions of a few Hertz, we determined that the range 3–6 was appropriate. These data in Fig. 2a are analyzed most easily using a maxima line plot, as shown in Fig. 2b, which is a two-dimensional graph of chemical shift vs. the scale of the wavelet transform. Maxima lines corresponding to real peaks cover a large range of scales on the scale-frequency plane. Examples are indicated by the asterisks next to

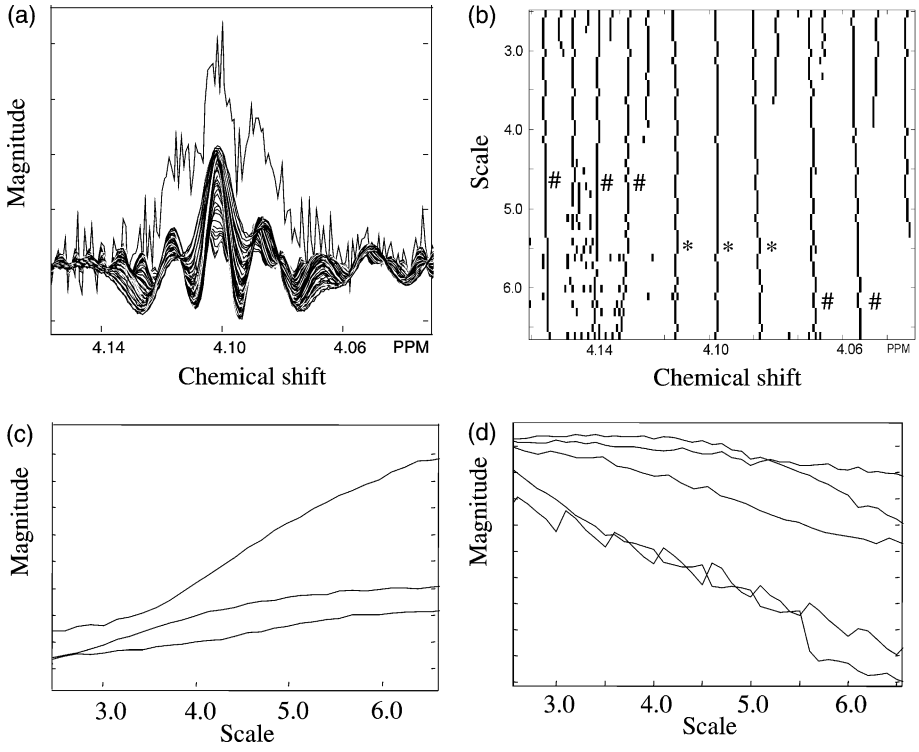

Fig. 2. (a) An expanded plot of the distorted triplet of sucrose with the CE current of 20 μA in Fig. 1, and the wavelet transforms of these peaks at different scales. (b) The maxima line plot of the data shown in (a). The maxima lines marked by * correspond to three line peaks and the truncated lines are caused by noise. The continuity of most of the lines related to noise is poor. However, five lines marked by # are continuous with scale but in fact correspond to noise. (c,d) Plots of the magnitude of the lines marked * and # vs. scale are able to differentiate between true lines and noise. In (c) the magnitude of the three maxima lines increases with scale, indicating that the peaks are real. In (d) the magnitude decreases with scale, indicating noise.

the lines in Fig. 2b. In contrast, noise typically appears as truncated maxima lines. It is possible for noise peaks to appear as continuous lines in the maxima plot, as indicated by the # symbols in Fig. 2b. In this case it is possible to distinguish between real signal and noise by analyzing the evolution of the magnitude of the lines as a function of scale. For real peaks the magnitude increases as a function of the scale, as shown in Fig. 2c, whereas for noise the magnitude decreases with scale, as shown in Fig. 2d. These two criteria can therefore be used to distinguish real signals from noise, effectively providing a degree of "denoising" to the spectrum.

Fig. 3 shows the results from a full current-distorted spectrum of sucrose with a CE current of 30 μA. This current produces substantial signal degradation in the sucrose spectrum, as shown in Fig. 3a. Compared to the sucrose spectrum obtained with no current applied, shown in Fig. 3b, the spectral linewidth of the residual HOD peak is broadened from 4.3 to 9.3 Hz. The results of reference deconvolution with a target linewidth of 4.3 Hz are shown in Fig. 3c. Fig. 3d shows the results obtained by using the complete algorithm described in this paper. Considerably more spectral information is available in the deconvolved spectrum than in the acquired spectrum in Fig. 3a. However, some fine multiplet structures which are present in a high-resolution spectrum acquired under ideal conditions are lost (see Section 4). The "noise-free" appearance of the final spectrum is artificial, since the output of the algorithm is a set of peaks, with associated linewidths and phases (the water peak is omitted from this final display since it contains no useful information).

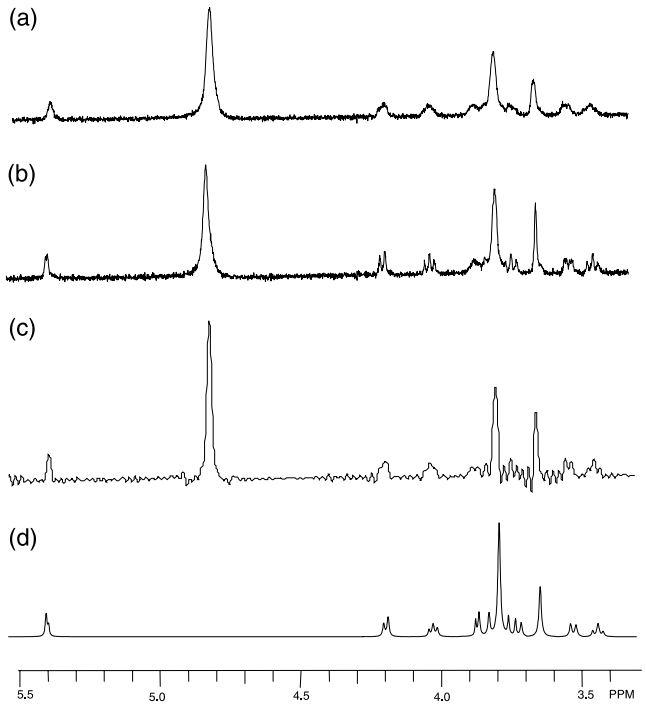

Fig. 3. (a) The spectrum of 100 mM sucrose in D_2O acquired with a current of 30 μA passing through the capillary. Number of complex data points: 6000, spectral width: 4000 Hz, the linewidth of the water resonance was 9.3 Hz. (b) Spectrum acquired with the current switched off. The linewidth of the water resonance was 4.3 Hz. (c) Spectrum produced using reference deconvolution with a target linewidth of 4.3 Hz. The frequency width of the reference region was set as 40 Hz around the water peak. (d) Spectrum obtained using the complete method described in this paper.

The HOD line as a reference for estimating the line broadening function is appropriate only at this small size scale. Previous results have shown that the temperature distribution over the fraction of sample that is situated within the RF coil is homogeneous [31]. At larger sizes, the well-known temperature sensitivity of the HOD resonance [32,33] would introduce a degree of line broadening unrepresentative of that of the solute.

4. Discussion

The field of hyphenated microseparations/NMR detection is a rapidly growing one, fueled by recent developments in small RF coil technology. Such coils have typically been of solenoidal geometry, due to the intrinsically high sensitivity. In the area of CE-NMR, however, solenoids suffer from intrinsically distorted NMR spectra due to the magnetic field gradients created by current flow in the sample. In this article, we have presented a data processing technique that can recover much of the spectral information: however, there are clear limitations. In cases where the current-induced line broadening is much larger than the frequency separation of the peaks, it is hard to restore spectral resolution using any processing technique, including the one detailed in this paper. The choice of parameters in the deconvolution process also involves some compromise between those that are best at resolving peaks that are close together in frequency and those that are optimal for peaks that are better resolved. For example, in the sucrose spectrum, it is possible to choose parameters that resolve the doublet-of-doublets at ~3.45 ppm. However, these parameters perform poorly for other sections of the spectrum. Comparing Figs. 3a and d certainly shows an increase in the information content of the spectrum, but care must be taken in spectral interpretation. Overall, the processing approach described herein provides an effective means to extract information from NMR spectra distorted by inhomogeneous magnetic fields. The demonstrated applicability of this methodology can be readily extended to a broad range of capillary electroseparations. In this manner, highest sensitivity NMR detectors can be coupled with highly efficient capillary electroseparations for on-line data acquisition.

Acknowledgments

We gratefully acknowledge the financial support of the National Institutes of Health (GM 53030). Partial support for this work was also provided by the National Science Foundation and the Alexander von Humboldt Foundation, Wolfgang Paul Preis.

References

[1] G.A. Morris, Compensation of instrumental imperfections by deconvolution using an internal reference signal, J. Magn. Reson. 80 (1988) 547–552.
[2] A. Gibbs, G.A. Morris, Reference deconvolution. Elimination of distortions arising from reference line truncation, J. Magn. Reson. 91 (1991) 77–83.
[3] G.A. Morris, D. Cowburn, Suppression of artefacts in nuclear Overhauser effect difference spectroscopy by reference deconvolution, Magn. Reson. Chem. 27 (1989) 1085–1089.
[4] A. Gibbs, G.A. Morris, A.G. Swanson, D. Cowburn, Suppression of t_1 noise in 2D NMR spectroscopy by reference deconvolution, J. Magn. Reson. A 101 (1993) 351–356.
[5] T.J. Horne, G.A. Morris, Combined use of gradient-enhanced techniques and reference deconvolution for ultralow t_1 noise in 2D NMR spectroscopy, J. Magn. Reson. A 123 (1996) 246–252.
[6] H. Barjat, G.A. Morris, S. Smart, A.G. Swanson, S.C.R. Williams, High-resolution diffusion-ordered 2D spectroscopy (HR-DOSY)—a new tool for the analysis of complex mixtures, J. Magn. Reson. B 108 (1995) 170–172.
[7] H. Barjat, G.A. Morris, A.G. Swanson, S. Smart, S.C.R. Williams, Reference deconvolution using multiplet reference signals, J. Magn. Reson. A 116 (1995) 206–214.
[8] G.A. Morris, Reference deconvolution in NMR, in: D.N. Rutledge (Ed.), Signal Treatment and Signal Analysis in NMR, Elsevier Science, Amsterdam, 1996, pp. 346–361.
[9] G.A. Morris, H. Barjat, T.J. Horne, Reference deconvolution methods, Prog. NMR Spectrosc. 31 (1997) 197–257.
[10] K.R. Metz, M.M. Lam, A.G. Webb, Reference deconvolution: a simple and effective method for resolution enhancement in nuclear magnetic resonance spectroscopy, Concepts Magn. Reson. 12 (2000) 21–42.
[11] N. Wu, T.L. Peck, A.G. Webb, R.L. Magin, J.V. Sweedler, Nanoliter volume sample cells for ^{1}H-NMR: application to on-line detection in capillary electrophoresis, J. Am. Chem. Soc. 116 (1994) 7929–7930.
[12] N. Wu, T.L. Peck, A.G. Webb, R.L. Magin, J.V. Sweedler, ^{1}H-NMR on the nanoliter scale: application to static and on-line measurements, Anal. Chem. 66 (1994) 3849–3857.
[13] K. Pusecker, J. Schewitz, P. Gfrorer, L.-H. Tseng, K. Albert, E. Bayer, On-line-coupling of capillary electrochromatography, capillary electrophoresis, and capillary HPLC with nuclear magnetic resonance spectroscopy, Anal. Chem. 70 (1998) 3280–3285.
[14] K. Pusecker, J. Schewitz, P. Gfrorer, L.-H. Tseng, K. Albert, E. Bayer, I.D. Wilson, N.J. Bailey, G.B. Scarfe, J.K. Nicholson, J.C. Lindon, On-flow identification of metabolites of paracetamol from human urine using directly coupled CZE-NMR and CEC-NMR spectroscopy, Anal. Commun. 35 (1998) 213–215.
[15] J. Schewitz, P. Gfrorer, K. Pusecker, L.-H. Tseng, K. Albert, E. Bayer, I.D. Wilson, N.J. Bailey, G.B. Scarfe, J.K. Nicholson, J.C. Lindon, Directly coupled CZE-NMR and CEC-NMR spectroscopy for metabolite analysis: paracetamol metabolites in human urine, Analyst 123 (1998) 2835–2837.
[16] D.L. Olson, M.E. Lacey, A.G. Webb, J.V. Sweedler, Nanoliter-volume ^{1}H-NMR detection using periodic stopped-flow capillary electrophoresis, Anal. Chem. 71 (1999) 3070–3076.
[17] P. Gfrorer, J. Schewitz, K. Pusecker, L.-H. Tseng, K. Albert, E. Bayer, Gradient elution capillary electrochromatography and hyphenation with nuclear magnetic resonance, Electrophoresis 20 (1999) 3–8.
[18] M.E. Lacey, R. Subramanian, D.L. Olson, A.G. Webb, J.V. Sweedler, High-resolution NMR spectroscopy of sample volumes from 1 nL to 10 μL, Chem. Rev. 99 (1999) 3133–3152.
[19] M.G. Khaledi (Ed.), High Performance Capillary Electrophoresis: Theory, Techniques, and Applications, Chemical Analysis: A Series of Monographs on Analytical Chemistry and Its Applications, vol. 146, Wiley, New York, 1998.
[20] J.P. Landers (Ed.), Handbook of Capillary Electrophoresis, second ed., CRC Press, Boca Raton, 1997.
[21] D.I. Hoult, R.E. Richards, The signal-to-noise ratio of the nuclear magnetic resonance experiment, J. Magn. Reson. 24 (1976) 71–85.
[22] P. Hoehl, Linear prediction spectral analysis of NMR data, Prog. NMR Spectrosc. 34 (1999) 257–299.
[23] H. Serrai, L. Senhadji, J.D. De Certaines, J.L. Coartieux, Time-domain quantification of amplitude, chemical shift, apparent relaxation time T_2 and phase by wavelet-transform analysis. application to biomedical magnetic resonance spectroscopy, J. Magn. Reson. 124 (1997) 20–34.
[24] D. Barache, J.-P. Antoine, J.-M. Dereppe, The continuous wavelet transform, an analysis tool for NMR spectroscopy, J. Magn. Reson. 128 (1997) 1–11.
[25] S. Ding, C.A. McDowell, High resolution, high sensitivity proton NMR spectra of solids obtained using continuous wavelet transform analysis, Chem. Phys. Lett. 322 (2000) 341–350.
[26] X. Shao, H. Gu, J. Wu, Y. Shi, Resolution of the NMR spectrum using wavelet transform, Appl. Spectrosc. 54 (2000) 731–738.
[27] S. Mallat, W.L. Hwang, Singularity detection and processing with wavelets, IEEE Trans. Information Theory 38 (1992) 617–643.
[28] S. Mallat, A Wavelet Tour of Signal Processing, Academic Press, San Diego, 1999.
[29] M.H. Hayes, Statistical Digital Signal Processing and Modeling, Wiley, New York, 1996.
[30] R.A. Kautz, M.E. Lacey, A.M. Wolters, F. Foret, A.G. Webb, B.L. Kargar, J.V. Sweedler, Sample concentration and separation for nanoliter-volume NMR spectroscopy using capillary isotachophoresis, J. Am. Chem. Soc. 123 (2001) 3159–3160.
[31] M.E. Lacey, A.G. Webb, J.V. Sweedler, On-line temperature monitoring in a CEC frit using microcoil NMR, Anal. Chem. 74 (2002) 4583–4587.
[32] J.C. Hindman, Proton resonance shift of water in gas and liquid states, J. Chem. Phys. 44 (1966) 4582–4592.
[33] A.G. Webb, Temperature measurement using nuclear magnetic resonance, Ann. Rep. NMR Spectrosc. 45 (2001) 1–67.